INTEGRATED OPTICAL CIRCUITS WITH SURFACE PLASMON POLARITONS

Elena VLĂDESCU[1]
Scientific coordinator: Prof. Univ. Dr. Daniela DRAGOMAN[2]

Abstract. *This thesis presents innovative contributions to the study of metal-dielectric-metal (MDM) integrated optical circuits with surface plasmon polaritons, using the transmission lines analogy for microwaves, the transfer matrix theory and the even-odd method. In the last chapter, I studied a plasmonic pulse to see how its shape changes when passing through waveguides with a variable number of periodic cells.*

Keywords: Plasmonics, metal-dielectric-metal, logic gate, slot waveguide

https://doi.org/10.56082/annalsarsciphyschem.2020.1.181

1. Introduction

Surface plasmon polaritons (SPPs) are non-radiative electromagnetic waves, confined to the interface of a metal with a dielectric, obtained following the interaction of light with the collective oscillations of free electrons in the metal. Their applications are in many important fields such as data storage, Raman spectroscopy, materials with negative refractive index at frequencies in the visible region, microscopy, solar cell fabrication, waveguides and the detection of biomolecules using sensors [1].

Integrated optical circuits could use SPPs for all the circuit's elements, which results in a miniaturization of circuits under the diffraction limit. SPPs can be used, for example, to fabricate very compact nanophotonic circuits and for optical interconnection on a motherboard. The study of integrated optical circuits with SPPs has many applications, which offer the possibility of theoretical investigation and practical realization of optical devices that can operate at the nanometric level [2].

2. Surface Plasmon Polaritons

Monochromatic transverse magnetic plasmonic waves (with frequency ω) are obtained at a metal-dielectric interface, as shown in Figure 1. This figure also illustrates the spatial distribution of the electric and magnetic fields of the SPP.

In agreement with the condition of continuity at the interface for the tangential components of the electric field, we find the dispersion relation of SPPs:

[1] PhD, Faculty of Physics, University Bucharest, 405 Atomistilor Street, Magurele, Romania
[2] Faculty of Physics, University of Bucharest, 405 Atomistilor Street, Magurele, Romania, and Academy of Romanian Scientists, 54 Splaiul Independentei, Bucharest, Romania.

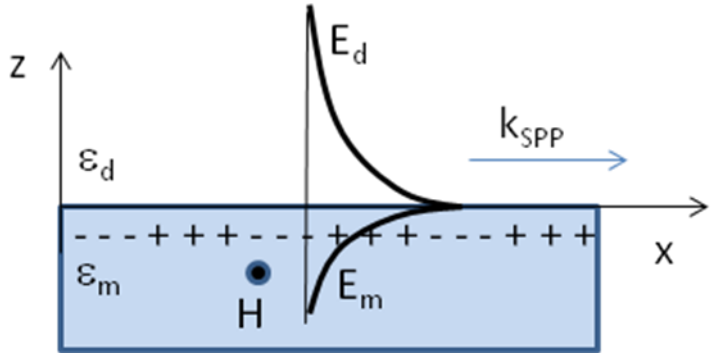

Fig. 1. Representation of the distribution of the components of the electromagnetic field of a plasmonic wave that appears at an interface between a metal and a dielectric

$$\varepsilon_d E_z^d = \varepsilon_m E_z^m \Rightarrow \quad k_{SPP}(\omega) = \frac{\omega}{c}\sqrt{\frac{\varepsilon_m(\omega)\cdot\varepsilon_d}{\varepsilon_m(\omega)+\varepsilon_d}} \tag{1}$$

If we graphically represent the dispersion relation (1) (see Figure 2), three areas of interest are distinguished: in the first domain $\omega < \omega_{SPP}$ for which $\varepsilon_m < -\varepsilon_d$ i.e. for frequencies ω lower than the resonance frequency of the surface plasmons ω_{SPP}, we have $k_{SPP} > k_0$ and the dispersion curve - represented by a black line, is below the curve corresponding to the incident radiation, i.e. to the curve $k_0 = \omega/c$ - marked with a black dotted line on the graph. The electromagnetic field of the SPPs decreases exponentially in the normal direction at the interface. The second domain is the one for which $\omega_{SPP} < \omega < \omega_P$, where ω_P is the plasma frequency. Here, in the absence of any loss, k_{SPP} has only an imaginary component, which means that the plasmonic wave does not propagate along the interface. The third domain is the one for which $\omega > \omega_P$, where we have volume plasmons. In the simulation we took $\varepsilon_d = \varepsilon_{air} = 1$, and $\lambda_0 = 0.632$ μm the wavelength of the electromagnetic radiation in vacuum. Regarding the permittivity of silver, this is described by the Drude-Lorentz model [3]. All simulations in this thesis were done with the Scilab open-source program. In all the simulations performed in this thesis, the losses were neglected and only the real part of the electrical permittivity dependence of frequency was considered:

$$\varepsilon_{re}(\omega) = 1 - \frac{\omega_P^2}{\omega^2} \tag{1}$$

where $\omega_P = ne^2/\varepsilon_0 m$ is the plasma frequency. In the case of silver, $\varepsilon_m = \varepsilon_{silver} = 1 - \omega_P^2/\omega^2$ with $\omega_P = 8.85\text{x}10^{15}$ Hz [3].

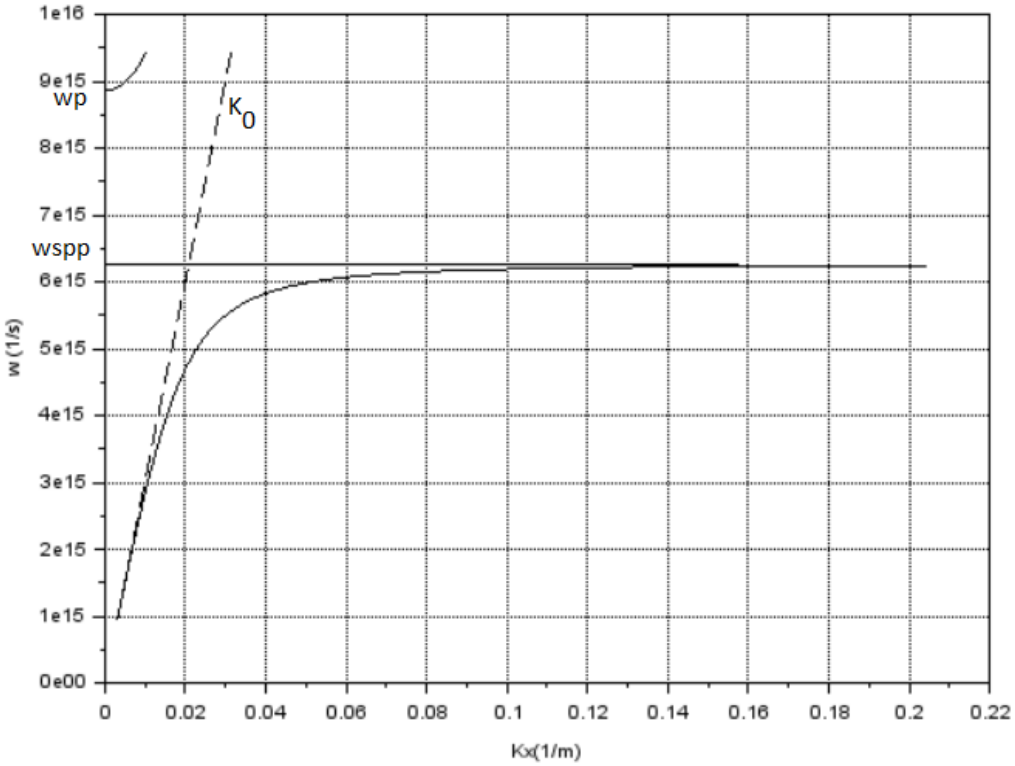

Fig. 2. Representation of the dispersion relation of the SPP for an air-silver interface

The propagation length of the SPP is given by:

$$L_{SPP} = 1/\mathrm{Im}(2k_{SPP}) \tag{3}$$

In practice, losses in conductors, called ohmic losses, limit the propagation length, which is a problem for the components of the SPP waveguides. The attenuation distances in dielectric and metal (for an attenuation of 1/e from the initial amplitude) are given by the relations:

$$d_d = \frac{\lambda}{2\pi}\sqrt{-\frac{\varepsilon_m + \varepsilon_d}{\varepsilon_d^2}} \qquad d_m = \frac{\lambda}{2\pi}\sqrt{-\frac{\varepsilon_m + \varepsilon_d}{\varepsilon_m^2}} \tag{4}$$

$\Rightarrow \varepsilon_d \cdot d_d = |\varepsilon_m| \cdot d_m$. Because $|\varepsilon_m| >> \varepsilon_d$, we can say that $d_m << d_d$.

In practice, d_m is about tens of nm and weakly depends on the wavelength λ, whereas d_d grows rapidly and nonlinearly with λ:

$$d_m \approx c/\omega_p \qquad d_d \approx (\lambda/2\pi)^2 \cdot (\omega_p / c\varepsilon_d) \tag{5}$$

SPPs cannot be produced directly because, for the same frequency, a phase mismatch occurs between the incident light vector k_0 and that of the plasmon-polariton denoted by k_{SPP}. Because we have $k_{SPP} > k_0$, this translates to the fact that SPPs cannot be excited by direct metal illumination. Various methods have been developed to overcome this mismatch, like Kretschmann configuration with a prism, Kretschmann configuration with a two-layer prism, difraction grating, microscope probe with scanning in near field SNOM or Otto configuration with a prism [1].

3. The Analogy with the Microwave Transmission Lines

MDM (metal-dielectric-metal) and DMD (dielectric-metal-dielectric) are the most common types of plasmonic waveguides, each having its characteristics, advantages and disadvantages [5]. Thus, in a MDM type waveguide, the magnetic field is more intense in the dielectric region and weaker in the metal region, because the plasmonic waves that appear at the two metal-dielectric interfaces overlap when the width of the guide is small, while in a DMD waveguide, we have the opposite situation. Thus, the magnetic field is located almost entirely inside the guide, with a minimum penetration depth outside the cross section of the MDM waveguide. In addition, the propagation length in MDM can exceed tens of microns for waveguides with widths less than 10% of the wavelength of vacuum light [4]. For DMD structures, the propagation length of the SPPs is of the order of centimeters for wavelengths in the near IR range, but the penetration depth of the SPPs is of the order of microns in the dielectric zone. [5]

Frequently MDM plasmonic waveguides are described by solving Maxwell equations by FDTD (finite difference time – domain) method, but this is time consuming. Another way to model SPP propagation through metal-dielectric-metal waveguides is to use the analogy with the microwave transmission lines. In this respect, it is possible to propose equivalent circuits for the MDM waveguides and to calculate the transmission through the waveguide, using the equations of the transmission lines.

In this thesis I studied various MDM configurations, including a single-arm MDM plasmonic waveguide, two MDM guides connected by a coupling section and an architecture consisting of two MDM waveguides, with an arm coupled perpendicular to the first guide. For example, the case of a single-arm MDM plasmonic waveguide is represented in figure 3, which indicates also the geometric parameters of the configuration.

If the dimensions of the waveguide and the arm comply with the conditions $h << \lambda$ and respectively $w << \lambda$, only one transversal TM mode will propagate through the waveguide.

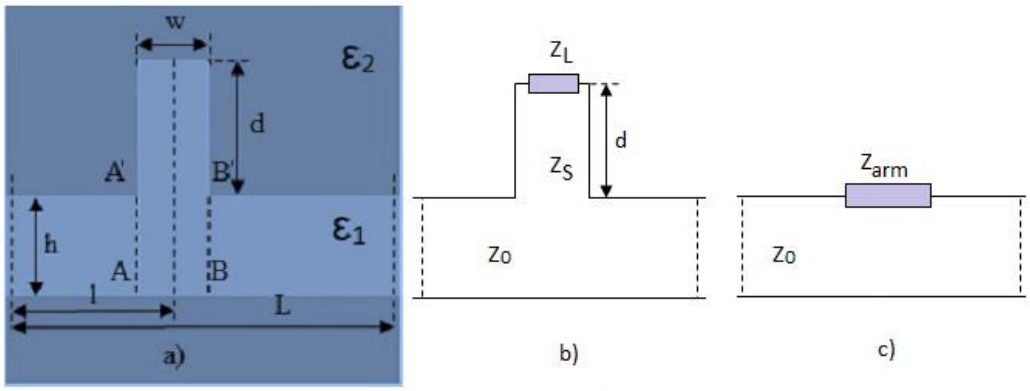

Fig. 3. (a) Schematic of a MDM waveguide with width h, with a single irregularity coupled perpendicular to the guide, length d and width w. (b) Representation of the circuit equivalent to (a) according to the transmission line theory and (c) its simplified representation

We can schematically represent the waveguide studied with a network consisting of an infinite transmission line with characteristic impedance Z_0 coupled in series with a finite transmission line with characteristic impedance Z_{arm} and we can write the transmittance at the end of the MDM guide using the transfer matrix analysis method, as the inverse of the square module of the element (1,1) of the total transfer matrix, $T = 1/|M_{11}|^2$:

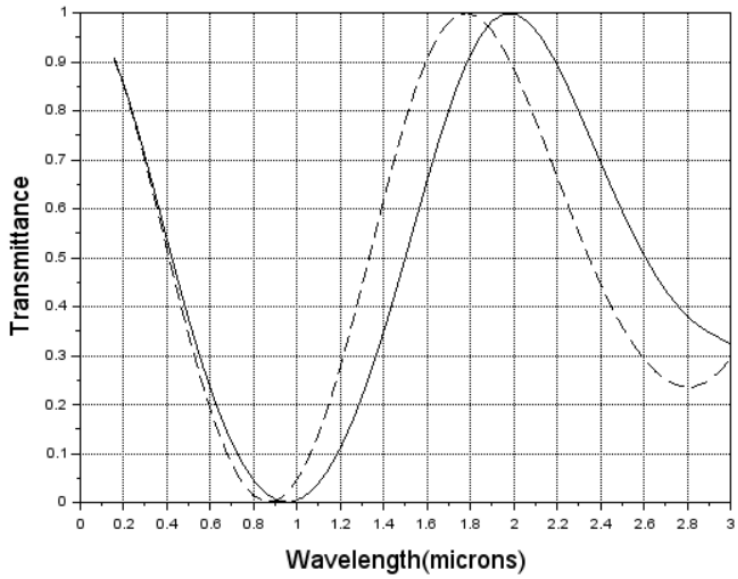

Fig. 4. Transmission curves for two Ag-air-Ag waveguides, one with an arm coupled perpendicular to the guide with ε = 1 (continuous line) as in the rest of the guide, and another with the arm with ε = 1.2 different from the rest of the guide (with dotted line)

$$T = \left| 1 + \frac{Z_{brat}}{2Z_0} \right|^{-2} \qquad M = A_1(l)BA_1(L-l) \tag{6}$$

where $A_1(l)$ is the matrix representing the propagation of SPPs through the waveguide with length l, B is the matrix representing the reflection of SPPs on the non-uniform section coupled perpendicular to the first guide, and $A_1(L\text{-}l)$ is the matrix that models the propagation of SPPs through the guide of length $L\text{-}l$.

I compared two transmission curves, one for an Ag-air-Ag waveguide with one arm coupled perpendicular to the waveguide with $\varepsilon = 1$ as in the rest of the guide, and another for a waveguide with one arm coupled perpendicular to guide with $\varepsilon = 1.2$ (see figure 4). From simulations, it turned out that the electrical permittivity and the arm length are the parameters that influence the position of the maximum transmittance, that is, we have a displacement of the curve towards smaller wavelengths when the electrical permittivity in the arm increases compared to the rest of the guide or, respectively, the arm length increases.

4. Plasmonic Logic Gates

For the implementation of some logic gates a MDM slot waveguide with constant section and one, two or three regions with variable electrical permittivity or different refractive index can be used (see Figure 5, which also indicates the dimensions of the configuration) [8]. Graphene can be embedded in the slot waveguide to obtain a variable permittivity region. This structure is reconfigurable. Reconfiguration involves applying another set of gate voltages on the three regions, without the need to change the dimensions of the guide.

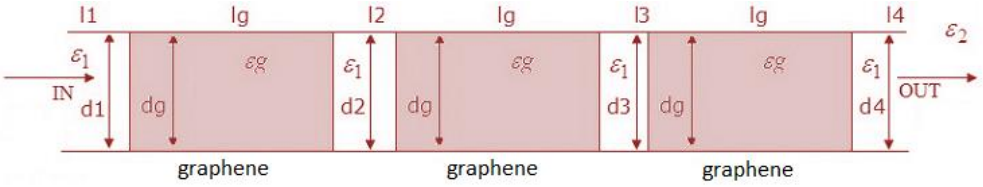

Fig. 5. MDM waveguide with three sections covered with graphene

For example, I simulated a three-bit Toffoli reversible universal logic gate using this structure. In this case, the first graphene region represents the first bit, with the logical input states 0 and 1, given by refractive indices corresponding to ε_{g0t} and ε_{g1t}, while the following two graphene sections represent control bits with values 0 and 1, encoded by the values of the refractive indices corresponding to ε_{g0c} and ε_{g1c}. I represented in the figure 6 the transmission coefficient as a function of the wavelength, for the following parameters of the structure: $l2 = l3 = lg1 = lg2 = lg3 = 100$ nm, $d1 = d2 = d3 = 40$ nm, $dg = 40$ nm, $\varepsilon_{g0t} = 1.2$, $\varepsilon_{g1t} = 5$ when

the first bit is 0 and ε_{g0c} = 4.75, ε_{g1c} = 1.2, that is, we represented states 000 (with black dashed line), 010 (with dash-dotted line), 001 (with dash-circle line) and 011 (with solid black line).

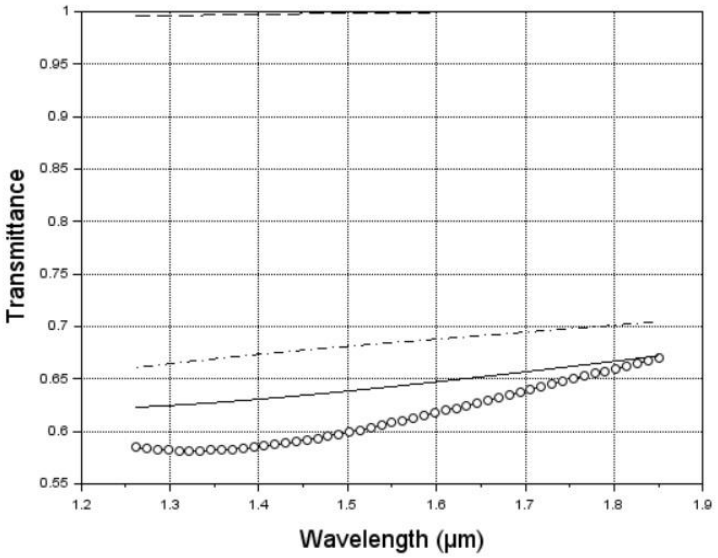

Fig. 6. Simulation of the Toffoli reversible universal logic gate for states 011 (with black dashed line), 010 (with dash-dotted line), 001 (with dash-circle line) and 000 (with solid black line)

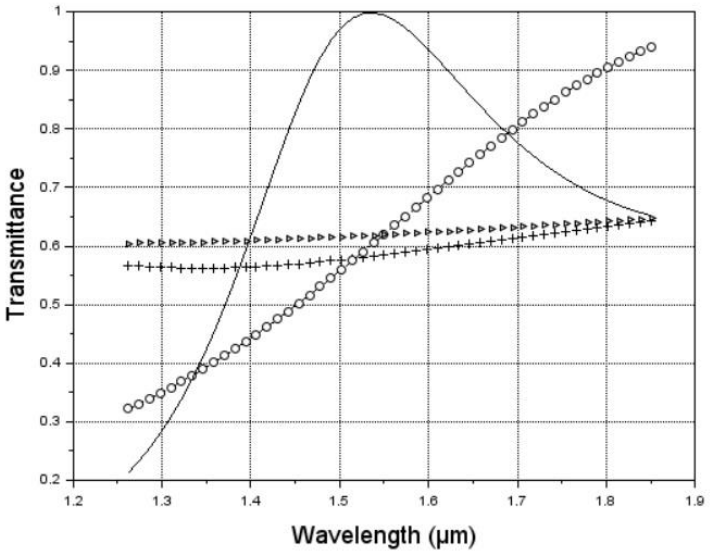

Fig. 7. Simulation of the Toffoli reversible universal logic gate for states 100 (+ black line), 110 (black dash-circle line), 101 (> black line) and 111 (black solid line)

In Figure 7, I represented the transmission coefficient as a function of the wavelength, for the following structure parameters: $l1 = l2 = l3 = l4 = lg1 = lg2 = lg3$ = 100 nm, $d1 = d2 = d3$ = 40 nm, dg = 40 nm, ε_{g0t} = 1.2, ε_{g1t} = 5 when the first

bit is 1 and ε_{g0c} = 1.2, ε_{g1c} = 4.75, that is, I represented states 100 (+ black line), 110 (black dash-circle line), 101 (> black line) and 111 (black solid line).

From these two figures it can be understand the operating principle of the Toffoli gate, which inverts the value of a bit when both control bits are 0. For this to happen, the value of transmittance T must have different values for 0 and 1 states. In this situation T is 0 for low transmittance, i.e. for $T < 0.7$ and 1 for $T > 0.9$ in Figure 6 and has opposite meaning in Figure 7. The transmittance changes from 0 to 1 state when the last bits are 11 in Figure 6, i.e. T is small for 000, 010 and 001 states and large for 011 state, and from 1 to 0 in Figure 7 if the last two bits are 11. The logic gate in these figures operates at 1.55 μm, which is an important wavelength in applications. Other logic gates can be implemented, for example CNOT, AND, OR if two graphene sections are activated by gate electrodes [8].

5. Ring Shaped Plasmonic Logic Circuits

The three- and four-port ring structures could function as various reversible and irreversible logic gates, if the amplitude and phase of the input signals are changed. The ring-type configurations studied in this thesis are symmetric to be able to use the even-odd analysis method of transmission lines [9]. For example, I investigated logical gates implemented through a symmetrical configuration with three ports like the one in Figure 8 [12].

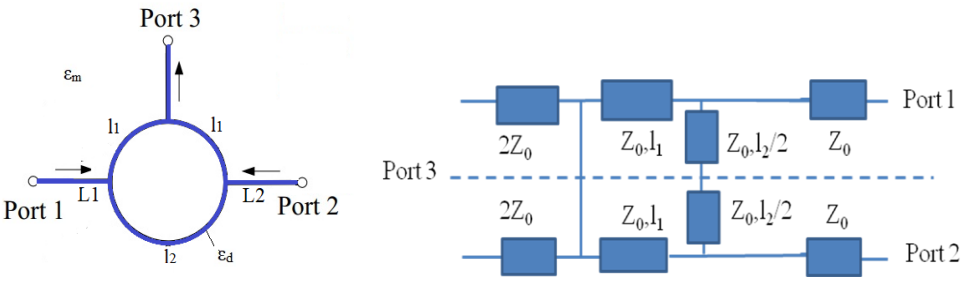

Fig. 8. MDM ring-shaped plasmonic waveguide, with three ports

a. Schematic representation b. Even-odd analysis equivalent circuit

The ring was chosen so that $l_2 = 2l_1$ and the input signals at ports 1 and 2 are a_1 and $a_2\exp\phi$, where a_1, a_2 are the amplitudes of the signals, ϕ is the relative phase between the two inputs, and the complex output signal from port 3 is denoted as t. The transmittance is $T = |t|^2$. The slot waveguide has a structure Ag/air/Ag, the relative dielectric constant of air is considered equal to 1, while the dielectric constant of the silver ε_m, is taken from [3]. In the following simulations was considered a waveguide with a width d = 50 nm, illuminated at λ_{exc} = 550 nm,

with k_{SPP} = 1.68x10^7 m^{-1} greater than $k_{exc} = 2\pi/\lambda_{exc}$ = 1.14x10^7 m^{-1}; the matching of the wave numbers and, implicitly, the excitation of SPPs can be done, for example, by means of a diffraction grating. In this case, we can replace the slot waveguide with a transmission line [6-7] with characteristic impedance given by:

$$Z_0 = \frac{k_{SPP} d}{k_{exc} c \varepsilon_d \varepsilon_0} = 27{,}6\,\mu\Omega \tag{7}$$

The transmittance T is a periodic function of the length l_1 (see Figure 9) for $a_1 = 1$, $a_2 = 1$, $\phi = 0$ (solid line), $a_1 = 1$, $a_2 = 0$ or $a_1 = 0$, $a_2 = 1$, regardless of ϕ (dashed line) and $a_1 = 1$, $a_2 = 1$, $\phi = \pi$ or $a_1 = 0$, $a_2 = 0$ (dashed-dotted line).

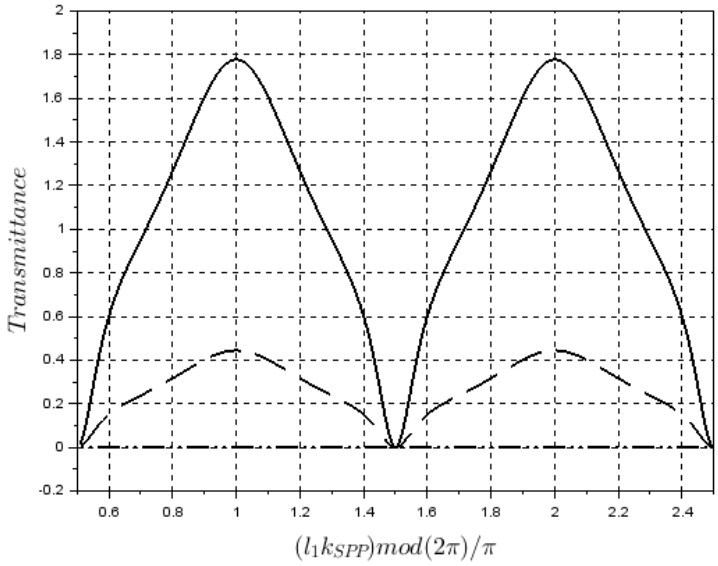

Fig. 9. Dependence of T on the dimensions of a 3-port ring circuit

Each time $l_1 k_{spp}$ is an integer multiple of π, the transmittance is maximum. This maximum is four times higher than in the case of a single input signal if the two inputs are in phase or disappear when the two inputs are out of phase (see Figure 9). This result can be analyzed by analogy with a ring-type acoustic gate [10], but in this case we measure intensities, and not acoustic amplitudes so that the variation of the signal from port 3 is much larger than in the acoustic case.

For a maximum T, suppose that $l_1 k_{SPP}$ is an integer multiple of π, and logical states 0 and 1 are encoded in the amplitudes of input states at ports 1 and 2. Then, as for the acoustic logic gate [10], the 3-port circuit implements the irreversible gate OR for $\phi = 0$ (the inputs in phase) if the output state is associated to logic values as follows: logic 1 for $T > 0.3$ and 0 otherwise. Indeed, in this case, as shown in

Figure 9, at output we have logic state 1 if one or both inputs are 1 logic and 0 if both are 0 logic. But there is a potential problem with the reading of output state: the transmittance has the same logic value for T about 1.8 when (a_1, a_2) = (1,1), and about 0.45 when (a_1, a_2) = (0,1) or (1,0). This very high difference between these output transmittances associated to logic state 1 can be attenuated through a different ϕ value. The phase difference ϕ can be changed by modifying the lengths of the input ports with $\Delta L = L_2 - L_1 = \phi/k_{SPP}$.

Similar, for $\phi = \pi$ (the inputs at ports 1 and 2 are out-of-phase), Figure 9 suggests that the circuit implements the XOR gate, which is an irreversible logic gate, for the same designation of the output state at port 3: T is associated to logic state 1 only for inputs (a_1, a_2) = (0,1) or (1,0).

If in figure 9 we associate the logic state 1 with $T > 1$ and the logic state 0 with $T < 1$, the circuit works as the gate AND, which is again an irreversible gate, for $\phi = 0$. In this situation the output state is 1 only when (a_1, a_2) = (1,1). Also, the configuration of the three-port slot waveguide studied above can implement the CNOT reversible logic gate.

I also studied the output intensity at port 4 of a four-port ring-shaped symmetrical waveguide, finding that the dependence of the output signal on the circuit's dimensions is more sensitive to their changes for the 4-port configuration than for a 3-port configuration. This is a situation that is not desirable because it imposes strict manufacturing tolerances. To avoid it, the 4-port circuit could be replaced by two 3-port ring-shaped plasmonic waveguides placed in cascade, for which the tolerances are more flexible [12].

6. Plasmonic Pulse Shaping

In this chapter is shown that the shape of a plasmonic pulse can also be changed using plasmonic circuits which consist of slot waveguides and arms, not only, as usual, by the controlled modulation of the spectral components of the optical pulse, which are spatially separated by gratings [11].

I studied a MDM slot waveguide, with the dielectric region having the width d and the electrical permittivity ε_d, and the metallic regions with the electrical permittivity ε_m. The waveguide has different arms attached in a periodic cell structure, the configuration of a single cell being represented in figure 10. The plasmonic circuit has N cells, each with two arms with the lengths l_1 and l_2 respectively at the distance L, and the widths are denoted by d_1 and d_2 respectively. The distance between the center of the second arm and the end of the cell is l, so that the distance between two groups of arms in adjacent cells is $\Delta L = l + d_1/2$.

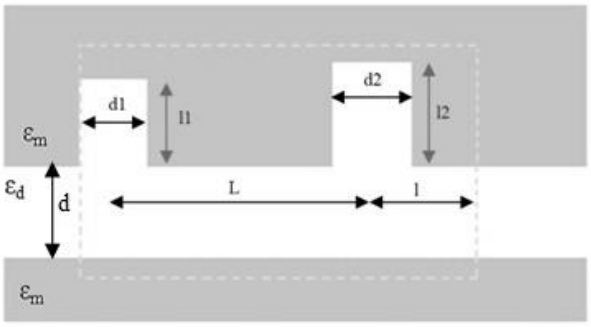

Fig. 10. The structure of a single cell

In order to obtain a much different shaped output pulse from that of the input pulse, the optical circuit must have a strongly frequency dependent transmission coefficient and the incident optical pulse should be as short as possible. I used the analogy with the microwave transmission lines [6-7] to describe each section of the waveguide length L through a matrix $A(L)$:

$$A(L) = \begin{pmatrix} \exp(-ik_{SPP}L) & 0 \\ 0 & \exp(ik_{SPP}L) \end{pmatrix} \tag{8}$$

and the impedance given by

$$Z_0 = k_{SPP}\, d / \omega \cdot \varepsilon_d . \tag{9}$$

For each arm j, where $j = 1, 2, \ldots$ the matrix M_j can be written as follows:

$$\begin{aligned} M_j &= \begin{pmatrix} 1 + Z_{a,j}/2Z_0 & -Z_{a,j}/2Z_0 \\ Z_{a,j}/2Z_0 & 1 - Z_{a,j}/2Z_0 \end{pmatrix} \\ Z_j &= k_{SPP,j} d_j / \omega\varepsilon_d \\ \phi_j &= k_{SPP,j} l_j \\ Z_{a,j} &= Z_j \frac{\sqrt{\varepsilon_d/\varepsilon_m} - i\tan\phi_j}{1 - i\sqrt{\varepsilon_d/\varepsilon_m}\tan\phi_j} \end{aligned} \tag{10}$$

where $k_{SPP,\,j}$ is the plasmon propagation constant through the arm width d_j, with j = 1.2. Also, I considered that $t(\omega) = 1/M_{11}$, where M_{11} is the element (1, 1) of the matrix that describes the plasmonic circuit, namely the matrix

$$M = [M_1 A(L) M_2 A(\Delta L)]^N \tag{11}$$

The simulations showed that the shape of the incident pulse can be changed by changing the dimensions of the circuit for a slot waveguide, with an Ag-air-Ag configuration, through which is transmitted a Gaussian input pulse $f(t) = \exp(-t^2/2\Delta t^2)$ with pulse duration Δt and the central frequency ω_0, corresponding to the wavelength of 800 nm and the width of the waveguide d = 70 nm. The circuit consisting of N cells modifies the pulse based on the following principle: The Fourier transform of the input pulse is multiplies by $t(\omega)$, so that the output pulse, obtained by taking an inverse Fourier transform, differs from the incident pulse.

For example, the left column of Figure 11 indicates with black dashed line the absolute value of the incident pulse, normalized to its maximum value, and with continuous black line the absolute value of the output pulse, while in the right column there are, the absolute values of the Fourier transforms for the input pulse (with black dashed lines) and the output pulse (with continuous black lines), normalized to the maximum of the Fourier transform of the incident pulse. The transmittance $T = |t|^2$ (blue line) is also indicated. This figure shows that the output pulse is shorter than the input pulse and has an asymmetric shape because the transmittance has a strong variation with frequency around ω_0. The output pulse is smaller than the incident pulse because of light reflection.

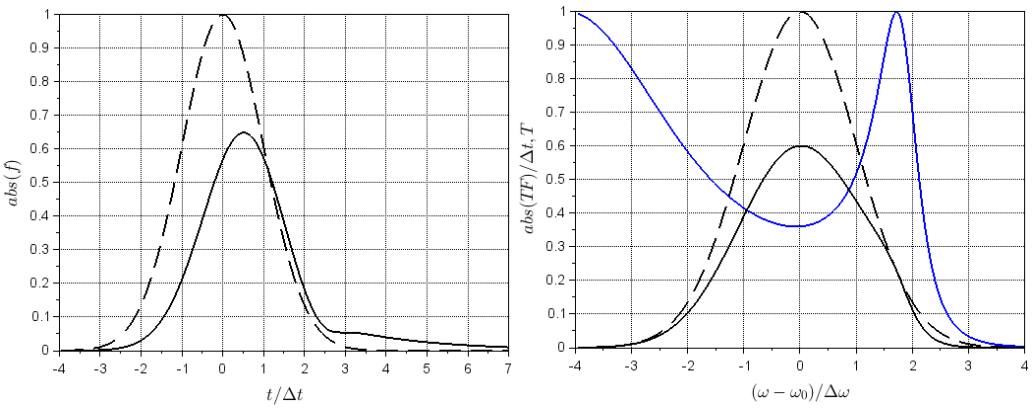

Fig. 11. Pulse evolution through the plasmonic circuit with Δt = 50 s, N = 3, d_1 = 75 nm, d_2 = 50 nm, l_1 = 450 nm, l_2 = 315 nm, L = 150 nm and ΔL = 200 nm

To study the influence of each parameter of the plasmonic circuit on the transmittance and, automatically, on the output pulse shape, I varied d_1, d_2, l_1, l_2, L, ΔL in turn and observed the effect of these variations on T and the shape of the pulse. From simulations it was observed that the most important parameter to modify if we want to change the output pulse is the length of the arms. For example, if we want to obtain a displacement with $\Delta\omega$ of the transmittance, we can, alternatively, vary by about 7% the distance between the arms, by about 9% the width of the arms or by about 0.4% their length. The applications of pulse

shaping at the exit of a plasmonic circuit range from microscopy, imaging, spectroscopy, high-speed communications to compressing optical pulses [18-23].

Conclusions

Surface plasmon-integrated optical circuits represent an alternative to electronic circuits [13-17] and have applications in fields such as waveguides, microscopy, data storage, Raman spectroscopy and biomolecules detection. Even though they are not as widespread today as electronic circuits, optical and especially plasmonic circuits are of interest because they can transmit information at higher speeds and, they are very compact.

The novelty of this thesis is the demonstration that architectures based on MDM slot waveguides can be used to implement logic gates, if they are excited by monochromatic radiation, or they can change the shape of light pulses. The simulations that prove these functionalities were based on the analogy with the microwave transmission lines and were performed using the open-source software Scilab.

It was shown that logic gates of the type NOT, OR, AND, CNOT and Toffoli can be implemented in a MDM plasmonic waveguide, with one, two or three sections covered by graphene. All of these logic gates are reversible and can be implemented in a single configuration containing three graphene regions whose refractive index can be adjusted independently using individually contacted gate electrodes. The results obtained in this chapter have been published in [8]. In all situations we have found that transmission can be strongly modulated, which is important for practical applications involving logic gates.

Innovative is also the use of analogy with the microwave transmision lines to demonstrate that ring-shaped, three- and four-port plasmonic slot waveguides can implement multiple logic gates with one, two and three bits depending on their configuration, amplitudes and phases of the input signals. These results have been published in [12]. In particular, we have shown that two ring structures with three ports can be cascaded in order to implement the universal and reversible CCNOT logic gate in a more efficient way than a similar ring structure, but with four ports.

Another original approach of this thesis concerns the demonstration of the possibility of adjusting the shape and the duration of an incident optical pulse when passing through plasmonic circuits consisting of periodic structures of arms. These changes are based on the different modulation of the amplitude and phase of the spectral components of the input pulse. We showed that the shape of the output pulse is influenced most by the variation of the arm length. These results are sent for publication. The particular importance of obtaining optical pulses with different shapes consists of possible applications in fields such as microscopy,

optical pulse compression, imaging, high speed communications and spectroscopy.

R E F E R E N C E S

[1] J. Zhang, L. Zhang, W. Xu, J. Phys. D, **45** (11), 113001 (2012).

[2] S. I. Bozhevolnyi, S. I. Bozhevolnyi, *Plasmonic Nanoguides and Circuits*. (Pan Stanford Publishing Pte. Ltd., Singapore, 2008).

[3] P. B. Johnson, R. W. Christy, Phys. Rev. B, **6**, 4370 (1972).

[4] R. Charbonneau, N. Lahoud, G. Mattiussi, P. Berini, Opt. Express **13**, 977 (2005).

[5] J. A. Dionne, L. A. Sweatlock, H. A. Atwater, Phys. Rev. B, **73** (3), 035407 (2006).

[6] A. Pannipitiya, I. D. Rukhlenko, M. Premaratne, H. T. Hattori, G. P. Agrawal, Opt. Express **18**(6), 6191 (2010).

[7] A. Pannipitiya, I. Rukhlenko, M. Premaratne, Photonics J., IEEE, **3** (2), 220 (2011).

[8] E. Vlădescu, D. Dragoman, Plasmonics, **13**, 2189 (2018).

[9] R. K. Mongia, I. J. Bahl, P. Bhartia, J. Hong, *RF and Microwave Coupled-Line Circuits*, 2nd ed., (Artech House, Boston, U.S.A, 2007).

[10] C. Zuo, J. Xia, H. Sun, Y. Ge, S. Yuan, X. Liu, Appl. Phys. Lett. **111**, 243501 (2017).

[11] A. M. Weiner, Opt. Commun. **284**, 3669 (2011).

[12] D. Dragoman, E. Vlădescu, Plasmonics **14**, 71 (2018).

[13] V. J. Sorger, R. F. Oulton, R. M. Ma, X. Zhang, MRS Bulletin **37**, 728 (2012).

[14] R. Kirchain, L. Kimerling, Nat. Photonics **1**, 303 (2007).

[15] D. A. B. Miller, Nat. Photonics **4**, 3 (2010).

[16] A. Boltasseva, H. A. Atwater, Science **331**, 290 (2011).

[17] F. Kusunoki, T. Yotsuya, J. Takahara, Opt. Express **14** (12), 5651 (2006).

[18] N. Dudovich, D. Oron, Y. Silberberg, Nature, **418**, 512 (2002).

[19] B. C. Chen, S. H. Lim, J. Phys. Chem. B, **112** (12), 3653 (2008).

[20] D. Oron, E. Tal, Y. Silberberg, Optics Express **13** (5), 1468 (2005).

[21] P. Schön, M. Behrndt, D. Aït-Belkacem, H. Rigneault, S. Brasselet, Phys. Rev. A **81** (1), 013809 (2010).

[22] T. W. Kee, M. T. Cicerone, Opt. Letters **29** (23), 2701 (2004).

[23] M. Muller, J. M. Schins, J. Phys. Chem. B **106** (14), 3715 (2004).